The EMBO Journal (2013) 32, 2287–2299
www.embojournal.org

TRANSPARENT PROCESS

THE EMBO JOURNAL

MAP1B-dependent Rac activation is required for AMPA receptor endocytosis during long-term depression

Marion Benoist[1], Rocío Palenzuela[1], Carlos Rozas[2], Patricio Rojas[2], Elena Tortosa[1], Bernardo Morales[2], Christian González-Billault[3], Jesús Ávila[1] and José A Esteban[1,*]

[1]Department of Neurobiology, Centro de Biología Molecular 'Severo Ochoa', Consejo Superior de Investigaciones Científicas (CSIC)/ Universidad Autónoma de Madrid (UAM), Madrid, Spain, [2]Department of Biology, Universidad de Santiago de Chile, Santiago, Chile and [3]Laboratory of Cell and Neuronal Dynamics, Department of Biology, Faculty of Sciences, Universidad de Chile, Santiago, Chile

The microtubule-associated protein 1B (MAP1B) plays critical roles in neurite growth and synapse maturation during brain development. This protein is well expressed in the adult brain. However, its function in mature neurons remains unknown. We have used a genetically modified mouse model and shRNA techniques to assess the role of MAP1B at established synapses, bypassing MAP1B functions during neuronal development. Under these conditions, we found that MAP1B deficiency alters synaptic plasticity by specifically impairing long-term depression (LTD) expression. Interestingly, this is due to a failure to trigger AMPA receptor endocytosis and spine shrinkage during LTD. These defects are accompanied by an impaired targeting of the Rac1 activator Tiam1 at synaptic compartments. Accordingly, LTD and AMPA receptor endocytosis are restored in MAP1B-deficient neurons by providing additional Rac1. Therefore, these results indicate that the MAP1B-Tiam1-Rac1 relay is essential for spine structural plasticity and removal of AMPA receptors from synapses during LTD. This work highlights the importance of MAPs as signalling hubs controlling the actin cytoskeleton and receptor trafficking during plasticity in mature neurons.

The EMBO Journal (2013) **32,** 2287–2299. doi:10.1038/emboj.2013.166; Published online 23 July 2013
Subject Categories: signal transduction; neuroscience
Keywords: LTD; MAP1B; Rac; Tiam

Introduction

Activity-dependent, long-lasting changes in synaptic strength are widely considered to be the cellular basis for learning and memory, and as such, they have been the subject of intense investigation. Within the postsynaptic terminal, it is now well established that an important mechanism for synaptic plasticity relies on the regulated addition or removal of AMPA-type glutamate receptors (AMPARs) at the synaptic membrane, in response to the activation of NMDA-type glutamate receptors (NMDARs) (Malinow and Malenka, 2002). Over the last two decades, detailed mechanistic knowledge has accumulated on the signalling cascades triggered upon NMDAR activation and the subsequent mobilization of AMPARs. In the case of long-term depression (LTD), Ca^{2+} entry through NMDARs leads to the activation of Ca^{2+}-sensitive phosphatases, such as calcineurin (Mulkey *et al*, 1993, 1994; Morishita *et al*, 2001), and endocytic factors, such as the small GTPase Rab5 (Brown *et al*, 2005), which mediate the clathrin-dependent internalization of AMPARs from the postsynaptic membrane (Beattie *et al*, 2000). Molecular rearrangements of the postsynaptic scaffold (Colledge *et al*, 2003; Horne and Dell'Acqua, 2007; Kim *et al*, 2007) and the actin cytoskeleton (Okamoto *et al*, 2004; Nakamura *et al*, 2011) are also key factors for LTD, possibly contributing to the coupling of structural and functional changes in the postsynaptic compartment. The small GTPase Rac1 has also been linked to LTD (Bongmba *et al*, 2011; Martinez and Tejada-Simon, 2011), possibly because of its role as a regulator of the actin cytoskeleton (Ridley, 2006).

In addition to the actin cytoskeleton, microtubules are also attracting considerable interest as potential regulators of synaptic function and plasticity. Besides providing long-range tracks along dendrites for the delivery of synaptic components, it has now been shown that microtubules transiently invade dendritic spines during periods of plasticity (Hu *et al*, 2008; Jaworski *et al*, 2009; Merriam *et al*, 2011). In addition, microtubule-associated proteins (MAPs) interact with a variety of other proteins, including F-actin, small G protein regulators and scaffolding molecules (Halpain and Dehmelt, 2006). Therefore, MAPs may potentially act as docking platforms for the localization and/or anchoring of important signalling molecules related to plasticity. These pleiotropic actions pose a challenge to discern developmental functions of these cytoskeletal elements during neuronal growth and synapse formation versus potentially more specialized roles for remodelling of established synapses during plasticity. We have addressed this particular problem for MAP1B.

MAP1B is the first MAP expressed during embryonic development of the nervous system (Schoenfeld *et al*, 1989). Consistent with its early expression, MAP1B plays critical roles in neurite growth and synapse development (Edelmann *et al*, 1996; Meixner *et al*, 2000; Gonzalez-Billault *et al*, 2004). MAP1B is required for both axon growth (Gonzalez-Billault *et al*, 2001, 2002; Tymanskyj *et al*, 2012) and spine maturation (Tortosa *et al*, 2011) in developing neurons. These functions are probably due to the capacity of MAP1B to modulate the activity of the small GTPases Rho and Rac1 via its interaction with specific guanosine nucleotide

*Corresponding author. Neurobiology, Centro de Biologia Molecular 'Severo Ochoa', Consejo Superior de Investigaciones Científicas (CSIC)/ Universidad Autónoma de Madrid, Nicolás Cabrera 1, Madrid 28049, Spain. Tel.: +34 91 1964637; Fax: +34 91 1964420;
E-mail: jaesteban@cbm.uam.es

Received: 10 December 2012; accepted: 2 July 2013; published online: 23 July 2013

exchange factors (GEFs), such as GEF-H1 and Tiam (Zhang and Macara, 2006; Kang *et al*, 2009; Montenegro-Venegas *et al*, 2010; Tortosa *et al*, 2011; Henriquez *et al*, 2012). However, the role of these pathways in specific forms of synaptic plasticity or their contribution to the orchestration of neurotransmitter receptor trafficking is unknown.

We investigated the specific role of MAP1B in the regulation of AMPAR trafficking during synaptic plasticity using a combination of molecular tools, together with electrophysiology and fluorescence imaging, on a mouse mutant expressing reduced levels of the MAP1B (Gonzalez-Billault and Avila, 2000). We found that MAP1B was indispensable for LTD expression, induced by either NMDARs or metabotropic glutamate receptors (mGluRs). Surprisingly, MAP1B was not required for the intracellular transport of AMPARs, but for their internalization from the synaptic membrane during LTD. We determined that MAP1B is necessary for the targeting of the Rac1 activator Tiam1 to the synapse. Accordingly, we observed that the LTD impairment in MAP1B-deficient neurons is due to insufficient Rac1 activation. Thus, proper synaptic plasticity can be restored by supplying additional Rac1 protein in these neurons. These new data provide basic insight into the regulation of AMPAR trafficking during synaptic plasticity, and underscore the role of MAPs as organizers of synaptic signalling in the spine.

Results

MAP1B is not required for the maintenance of basal synaptic function

As the first step in evaluating the role of MAP1B in synaptic transmission, we tested basal synaptic properties in heterozygous MAP1B mutant mice expressing roughly 50% of the normal protein levels (Gonzalez-Billault *et al*, 2000). These mice express normal levels of other MAPs, such as MAP1A, MAP2, MAP4, tau and LC3, as well as α-tubulin, βII-tubulin and β-actin (Gonzalez-Billault *et al*, 2000). Homozygous MAP1B-deficient mice die during the first postnatal day, probably due to severe alterations of the nervous system during embryonic development. In contrast, heterozygous mice survive to adulthood and they do not present any overt abnormality (Gonzalez-Billault *et al*, 2000). Therefore, these mice offer an ideal opportunity to test the effect of limiting amounts of MAP1B on mature neurons.

Acute hippocampal slices were prepared from 2- to 3-week-old MAP1B+/− mice and wild-type littermates as a control. The effect of decreased MAP1B expression was evaluated using whole-cell recordings from CA1 neurons, under voltage-clamp configuration, stimulating presynaptic Schaffer collaterals. As shown in Figure 1A, decreased MAP1B levels did not produce a significant difference in the ratio between synaptic responses mediated by AMPARs and NMDARs (AMPA/NMDA ratio) compared to wild-type animals (AMPA and NMDA responses were measured at −60 and +40 mV, respectively, in the presence of the $GABA_A$ receptor antagonist, picrotoxin). The ratio between AMPA and GABA responses was similarly unaffected (AMPA and GABA responses were measured at −60 and 0 mV, respectively, in the presence of the NMDAR antagonist, AP-V; Figure 1B). Other passive membrane properties, such as input resistance and holding current, were not altered in MAP1B+/− mutant neurons (Supplementary Figure 1).

To further evaluate the role of MAP1B in basal synaptic transmission, we carried out input/output experiments. We measured the slope of the field excitatory postsynaptic potential (fEPSP) recorded from the *stratum radiatum* of CA1, as a function of the stimulation intensity applied to the Schaffer collateral fibres. As shown in Figure 1C, the input/output curves of wild-type and MAP1B+/− slices were similar. These results indicate that MAP1B expression levels are not limiting for postsynaptic function under basal conditions.

MAP1B is required for proper axonal growth (Gonzalez-Billault *et al*, 2001). Therefore, we evaluated whether presynaptic properties would be altered in acute slices from MAP1B heterozygous animals. Paired-pulse facilitation (Figure 1D) and post-tetanic potentiation (PTP) (Figure 1E and F) were not altered in heterozygous MAP1B slices, compared to wild type. These combined results support the idea that MAP1B is not a limiting factor for presynaptic function in CA3-to-CA1 synaptic transmission.

MAP1B deficiency enhances LTP

To evaluate the potential role of MAP1B in synaptic plasticity, long-term potentiation (LTP) was induced with a high-frequency stimulation (HFS) protocol (100 Hz, 1 s, four times separated by 10 s) in hippocampal slices from wild-type and heterozygous MAP1B mutants. The extent of potentiation was compared across the animals. As shown in Figure 2A and B, the potentiation observed was not significantly different between MAP1B mutant (160 ± 16%) and wild-type mice (170 ± 20%).

In order to avoid potential ceiling effects of LTP expression with HFS, we tested a theta-burst stimulation (TBS) protocol, which is considered as more physiological (TBS: 5 trains, each with 10 bursts at 5 Hz, each burst containing 4 pulses at 100 Hz). As shown in Figure 2C and D, MAP1B+/− slices yielded significantly more potentiation than wild-type slices (209 ± 11% versus 140 ± 6%). Therefore, LTP is enhanced in MAP1B+/− mutant slices when a weaker LTP protocol is used.

To further evaluate this point, we again tested the HFS protocol, but under conditions in which LTP induction is attenuated, by increasing extracellular Mg^{2+} concentration. As shown Figure 2E and F, LTP is completely abolished in wild-type slices with this protocol (120 ± 18%), whereas there is still a significant potentiation in MAP1B heterozygous slices (200 ± 32%). These combined results indicate that LTP is facilitated in MAP1B-deficient neurons.

MAP1B is required for LTD

The facilitation of LTP observed above suggests that there may be a shift in synaptic plasticity in MAP1B+/− neurons. To explore this possibility, we tested LTD expression in MAP1B-deficient slices. NMDAR-dependent LTD was induced with 1 Hz stimulation for 15 min, while recording fEPSP in CA1 *stratum radiatum*. As shown in Figure 3A and B, this protocol induced a strong depression in wild-type slices (33 ± 11% depression). In contrast, MAP1B+/− slices failed to show any depression.

In order to test if this phenotype was restricted to NMDAR-dependent LTD, we evaluated mGluR-dependent LTD induced by application of 50 μM DHPG ((S)-3,5-dihydroxyphenylglycine, a specific agonist of group I mGluRs). As shown in Figure 3C and D, DHPG led to a significant depression in

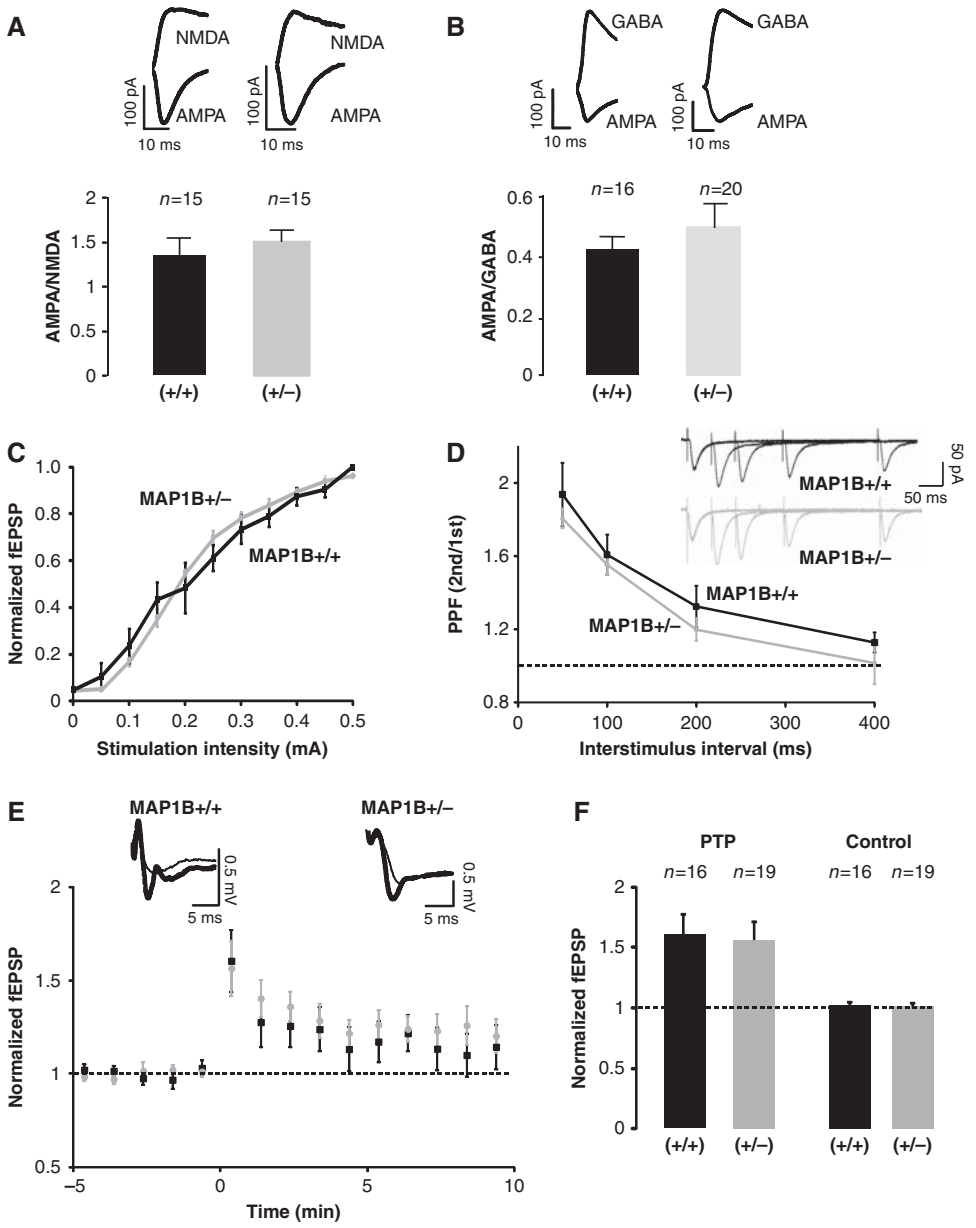

Figure 1 Effect of reduced MAP1B expression levels on pre- and postsynaptic properties of synaptic function. (**A**) AMPA/NMDA ratios were calculated from synaptic responses recorded in patch-clamp configuration in the presence of picrotoxin at −60 mV for AMPARs and +40 mV for NMDARs (NMDA responses are collected at a latency of 100 ms). '*n*' represents the number of cells (typically from 4 to 6 animals). Black column represents MAP1B+/+ and grey column represents MAP1B+/−. (**B**) AMPA/GABA ratios were recorded in the presence of APV at −60 mV for AMPA and 0 mV for GABA. '*n*' represents the number of cells. Black column for MAP1B+/+ and grey column for MAP1B+/−. (**C**) Input–Output relations from field EPSPs at different stimulation intensities. fEPSP values are normalized to the average response obtained with wild-type mice at 500 μA. Black squares represent MAP1B+/+ and grey circles represent MAP1B+/−. (**D**) Paired-pulse facilitation ratios from whole-cell synaptic responses evoked by stimulation of the Schaffer collateral fibres with different interstimulus intervals (50, 100, 200 and 400 ms). Inset: representative traces of the paired-pulse facilitation experiment from MAP1B+/− (grey) and wild-type (black) littermates. (**E**) Time course of fEPSPs recorded from CA3-to-CA1 synapses during post-tetanic potentiation (PTP: stimulation at 100 Hz for 1 s, in the presence of 100 μM AP-V). Black squares represent MAP1B +/+ and grey circles represent MAP1B+/−. (**F**) Average fEPSP responses collected 2 min after PTP induction and normalized to the baseline. Left columns (PTP) correspond to the induced pathway (100 Hz, 1 time). Right columns (Controls) correspond to the pathway that was not stimulated during the induction; '*n*' represents the number of slices. Both wild-type (black) and MAP1B+/− (grey) slices were significantly potentiated with respect to their baseline ($P=0.003$ and $P=0.005$, respectively, according to the Wilcoxon test).

wild-type slices (32 ± 9% depression), whereas no depression was observed in MAP1B+/− slices.

To check whether this defect in LTD expression was due to developmental alterations in the MAP1B+/− mice, we acutely downregulated MAP1B expression in wild-type mouse neurons using an shRNA approach. As shown in Figure 3E and F, MAP1B expression can be efficiently knocked down using lentiviral-driven expression of a specific shRNA in organotypic hippocampal slice cultures from wild-type mice. Under these conditions, LTD expression was also strongly impaired, whereas a scrambled shRNA control had no effect (Figure 3G and H). These results indicate that

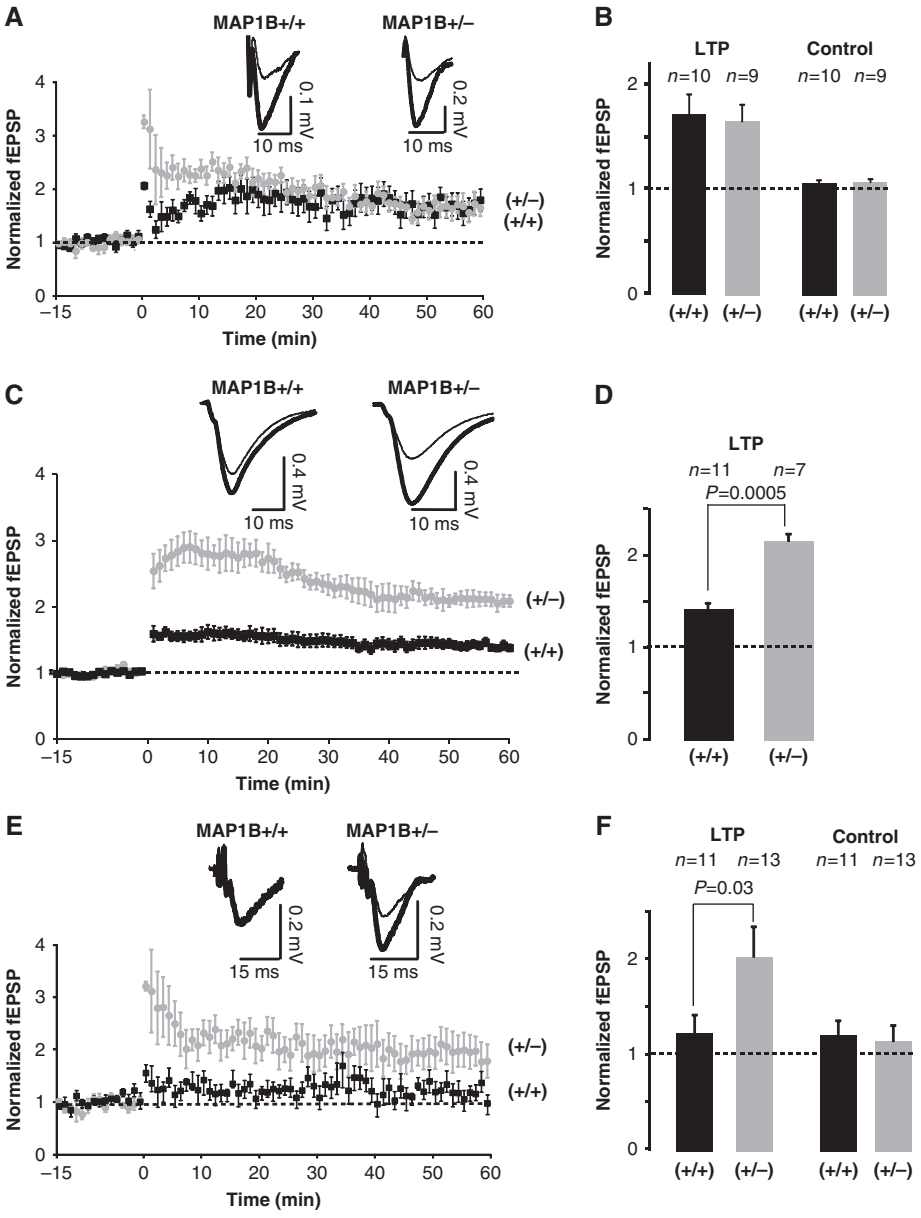

Figure 2 Effect of MAP1B deficiency on LTP expression. fEPSPs were recorded from CA3-to-CA1 synapses and normalized to the average baseline value before LTP induction. (**A**) Time course of HFS LTP induction (100 Hz for 1 s, 4 times separated by 10 s) from MAP1B+/+ and MAP1B+/− slices. (**B**) Average responses collected from the last 5 min of the recording and normalized to the baseline. Left columns (LTP) correspond to the induced pathway. Right columns (Control) correspond to the pathway that was not stimulated during the induction. Both wild-type and MAP1B+/− slices were significantly potentiated with respect to their baselines ($P=0.01$ and $P=0.008$, respectively, according to the Wilcoxon test). (**C**) Time course of TBS LTP induction (5 trains of 10 bursts at 5 Hz each, 1 burst = 4 pulses at 100 Hz) from MAP1B+/+ and MAP1B+/− slices. (**D**) Average responses collected from the last 5 min of the recording and normalized to the baseline. Both wild-type and MAP1B+/− slices were significantly potentiated with respect to their baselines ($P=0.004$ and $P=0.02$, respectively, Wilcoxon test). (**E**) Time course of HFS LTP (100 Hz for 1 s, 4 times separated by 10 s), in the presence of 2 mM Ca^{2+}, 2 mM Mg^{2+} (1:1 Ca^{2+}/Mg^{2+} ratio) from MAP1B+/+ and MAP1B+/− slices. (**F**) Average responses collected from the last 5 min of the recording and normalized to the baseline. Left columns (LTP) correspond to the induced pathway. Only MAP1B+/− slices were significantly potentiated with respect to their baseline ($P=0.003$, Wilcoxon test). Right columns (Control) correspond to the pathway that was not stimulated during the induction. For all panels, '*n*' represents the number of slices and '*P*' the statistical significance value comparing the extent of potentiation in wild-type (black squares) versus MAP1B+/− (grey circles) slices (Mann–Whitney test).

MAP1B is acutely required for this form of synaptic plasticity, and not just as a developmental adaptation.

These combined results suggest that MAP1B is a strict limiting factor for LTD expression. On the other hand, the fact that both NMDAR- and mGluR-dependent LTD behave in the same manner, suggests that MAP1B is involved in AMPAR synaptic removal (common to both NMDAR and mGluR LTD) instead of specific NMDAR or mGluR downstream signalling.

MAP1B is required for AMPAR endocytosis and spine shrinkage during LTD

To determine the mechanism by which the decrease in MAP1B levels abolishes LTD, we examined the endocytosis of AMPARs upon NMDAR activation. Organotypic hippocampal slices were prepared from wild-type and MAP1B+/− animals, and GluA2 tagged with a pH-sensitive form of GFP (SEP-GluA2; Makino and Malinow, 2009) was expressed together

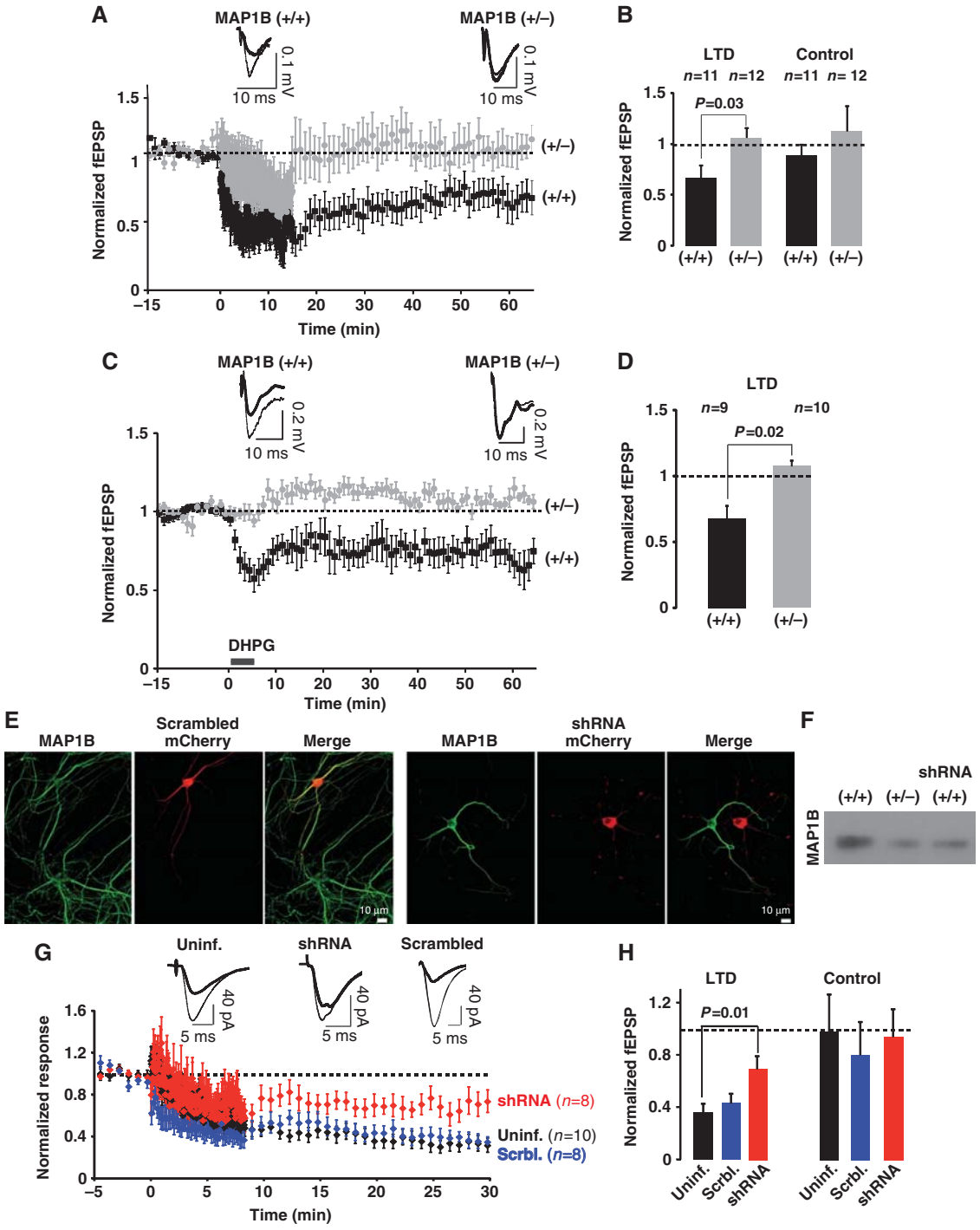

Figure 3 Effect of MAP1B deficiency on LTD expression. fEPSPs were recorded from CA3-to-CA1 synapses and normalized to the average baseline value before LTD induction. (**A**) Time course of NMDAR-dependent LTD (1 Hz, 15 min) from MAP1B+/+ and MAP1B+/− slices. (**B**) Average responses collected from the last 5 min of the recording and normalized to the baseline. Left columns (LTD) correspond to the induced pathway. Only wild-type slices were significantly depressed with respect to their baseline ($P = 0.03$, Wilcoxon test). Right columns (Control) correspond to the pathway that was not stimulated during the induction. (**C**) mGluR LTD was induced in MAP1B+/+ and MAP1B+/− slices with 50 µM of (RS)-3,5-DHPG for 5 min, as indicated. (**D**) Average responses collected from the last 5 min of the recording and normalized to the baseline. MAP1B+/+ slices were significantly depressed with respect to their baseline ($P = 0.03$, Wilcoxon test). For all panels, '*n*' represents the number of slices and '*P*' the statistical significance value comparing the extent of depression in wild-type (black squares) versus MAP1B+/− (grey circles) slices (Mann–Whitney test). (**E**) Immunofluorescence images of MAP1B expression levels (green) and mCherry (red, lentiviral infection) from hippocampal primary neuronal cultures expressing the MAP1B shRNA (right panels) or the scrambled control (left panels). (**F**) Western blot showing the expression levels of MAP1B in organotypic slices from wild-type and heterozygous (MAP1B+/−), and from wild-type animals after the expression of the shRNA against MAP1B. (**G**) Time course of NMDAR-dependent LTD (500 pulses at 1 Hz) on wild-type organotypic hippocampal slice cultures from control (uninfected) neurons, neurons expressing a scrambled shRNA or from neurons expressing the shRNA against MAP1B, as indicated. (**H**) Average responses collected from the last 5 min of the recording and normalized to the baseline. Left columns (LTD) correspond to the induced pathway. Right columns (Control) correspond to the pathway that was not stimulated during the induction.

with a cytosolic red fluorescence protein (Tomato) (Figure 4A and D; see Materials and methods). The level of GluA2 receptors at the spine surface was followed during a 'chemical LTD' experiment (cLTD: 20 μM NMDA, 5 min) by quantifying SEP fluorescence in the spine compared to the adjacent dendritic shaft, using live-imaging confocal microscopy. Before LTD induction, SEP-GluA2 accumulation in spines was comparable in wild-type and MAP1B+/− neurons (Figure 4B). This result is consistent with the similar basal synaptic transmission observed in wild-type and mutant slices (Figure 1). In addition, neither spine size (see below, Figure 5G and H, and Supplementary Figure 3D and E) nor long-range dendritic trafficking of SEP-GluA2 (Supplementary Figure 2A and B) was altered in MAP1B+/− neurons.

As expected, cLTD induction produced a sustained reduction in SEP-GluA2 fluorescence in the spines from wild-type neurons (Figure 4A–C), indicating that GluA2 receptors were removed from the surface of the spine. In contrast, SEP-GluA2 fluorescence did not significantly change in MAP1B+/− neurons, suggesting that GluA2 receptors failed to be internalized and remained at the spine surface during and after LTD induction.

In addition to AMPAR removal, it has been reported that LTD induction produces a reduction in spine size (Zhou *et al*, 2004). Therefore, we tracked changes in spine size during LTD in wild-type and MAP1B+/− neurons. To this end, we monitored Tomato fluorescence as a volume indicator. As shown in Figure 4D and E, NMDA application produced a fast decrease in Tomato fluorescence in the spine of wild-type neurons, indicating that NMDA treatment induces rapid and long-lasting spine shrinkage in wild-type neurons. In contrast, in MAP1B+/− neurons, only a slight decrease (5–10%) in Tomato fluorescence in the spine followed NMDA application. The difference with respect to wild-type neurons is particularly noticeable in the population of spines under-

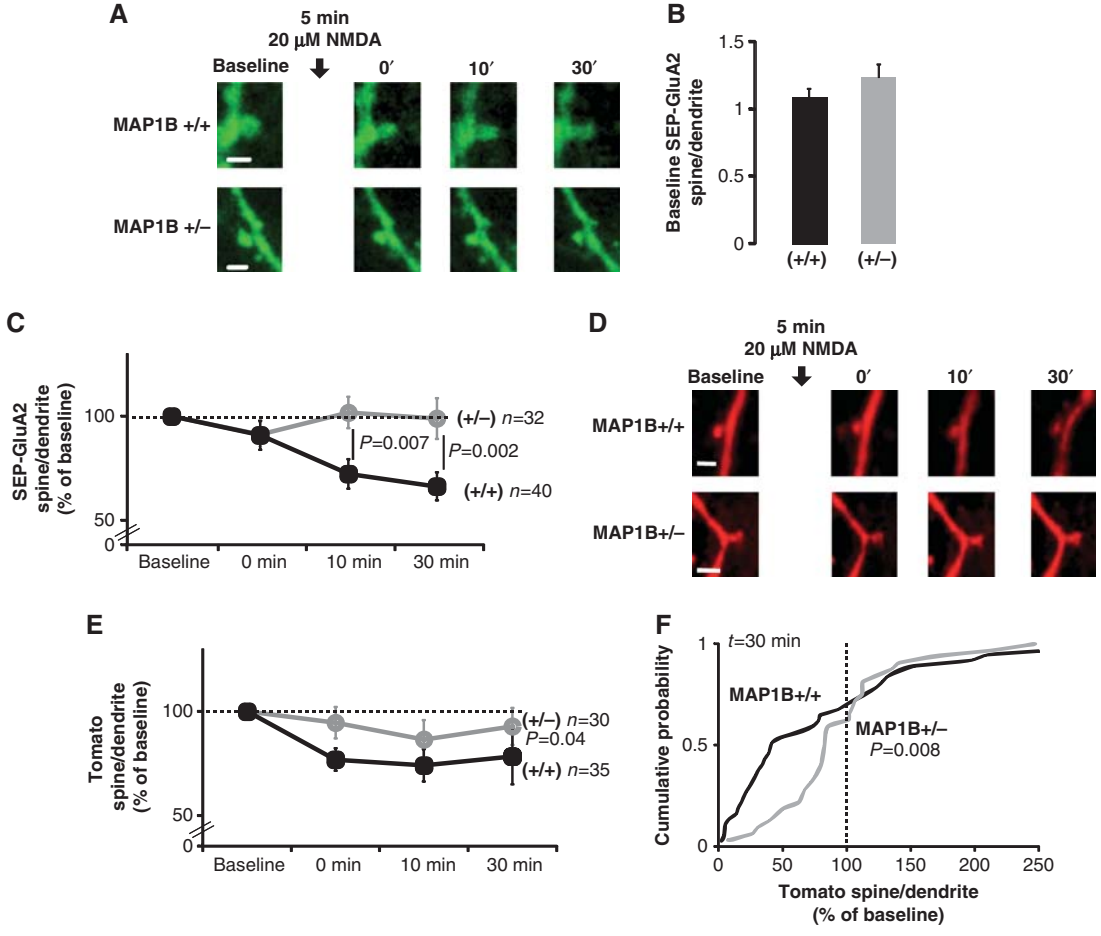

Figure 4 AMPAR endocytosis and spine shrinkage in MAP1B-deficient neurons. (**A**) Representative confocal images of dendritic spines from CA1 neurons of wild-type and MAP1B+/− organotypic hippocampal slice cultures expressing SEP-GluA2. Images were acquired before (Baseline) and at different times after cLTD induction (black arrow, 20 μM NMDA). Scale bar: 2 μm. (**B**) Spine/dendrite ratios of SEP-GluA2 for wild-type and MAP1B+/− neurons before cLTD induction (Baseline). (**C**) Time course of SEP-GluA2 spine/dendrite ratios normalized to the baseline value. There was a significant decrease in SEP-GluA2 spine/dendrite ratio compared to baseline for wild-type neurons ($P=0.0001$ at 10 min and $P<0.0001$ at 30 min; Wilcoxon test). '*n*' represents the number of spine–dendrite pairs. '*P*' represents the statistical significance value when comparing SEP-GluA2 changes between wild-type and MAP1B+/− neurons (Mann–Whitney test). (**D**, **E**) Similarly to (**A**) and (**C**), monitoring Tomato fluorescence as an indicator of spine/dendrite volumes. There was a significant decrease in Tomato spine/dendrite ratio compared to baseline for wild-type neurons ($P=0.0007$ at 0 min after cLTD induction, $P=0.002$ at 10 min, and $P=0.009$ at 30 min; Wilcoxon test). (**F**) Cumulative probability distributions of normalized changes in Tomato spine/dendrite ratios 30 min after cLTD induction. Vertical dashed line at 100% represents no change in spine/dendrite ratio with respect to the baseline. '*P*' represents the statistical significance value comparing wild-type and MAP1B+/− neurons (Kolmogorov–Smirnov test). For all panels, black is for wild type and grey for MAP1B+/−.

going size reduction (those with a spine/dendrite ratio of <100% of the baseline; see cumulative distribution in Figure 4F). The shrinkage of this population of spines was significantly attenuated in MAP1B+/− neurons (rightward displacement in spine/dendrite ratios <100%). To note, for both wild-type and MAP1B+/− neurons, the reduction in spine size is larger than the decrease in AMPA receptor content, which leads to an increase in the ratio of SEP-GluA2/Tomato in the spine (Supplementary Figure 2C).

In conclusion, these combined data indicate that the reduction in MAP1B levels impairs both spine structural plasticity and AMPAR internalization during LTD.

MAP1B deficiency alters actin accumulation in spines

The alteration in spine structural plasticity in MAP1B-deficient neurons suggests that the actin cytoskeleton may be involved. Hence, we decided to evaluate the actin accumulation in spines from wild-type and MAP1B-deficient mutant mice. To this end, we expressed EGFP-actin in organotypic hippocampal slices. EGFP fluorescence was quantified in spines and compared to fluorescence in the adjacent dendrite shafts (spine/dendrite ratio). As shown in Figure 5A–C, actin accumulation in spines was significantly higher in MAP1B+/− neurons compared to wild type.

This difference in actin concentration may be a passive consequence of difference in spine size. Therefore, we compared spine morphology and density between wild-type and MAP1B+/− neurons. To this end, we perfused 2-month-old animals with fixative, and revealed neuronal structure by filling-in CA1 neurons with Alexa 594 (see Materials and methods). As shown in Figure 5D–F, there was no significant difference in spine density or spine head diameter (Figure 5G and H) in apical dendrites from wild-type of MAP1B+/− animals (similar results were obtained with basal dendrites; Supplementary Figure 3). Therefore, we conclude that the enhanced accumulation of actin in MAP1B+/− spines is not linked to changes in spine size, but may be caused by alterations in the regulation of the actin cytoskeleton.

Tiam1-Rac1 deficits are responsible for LTD impairment in MAP1B-deficient neurons

We have previously shown that MAP1B interacts with the Rac1 activator Tiam1 (Montenegro-Venegas *et al*, 2010; Tortosa *et al*, 2011; Henriquez *et al*, 2012), which has been linked to spine morphogenesis (Zhang and Macara, 2006). Therefore, we investigated whether alterations in Tiam1-Rac1 would be involved in the synaptic deficits of MAP1B mutant neurons.

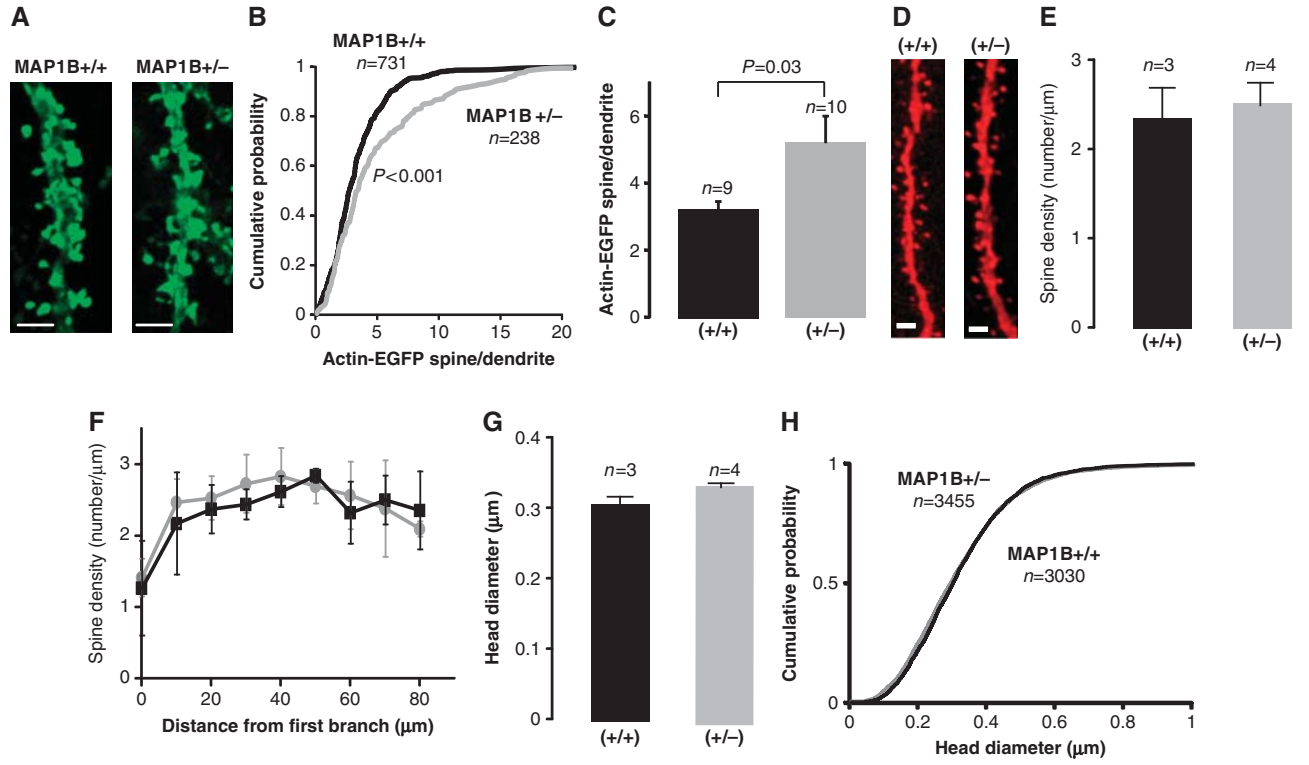

Figure 5 Actin accumulation and spine morphology in MAP1B-deficient neurons. (**A**) Representative confocal images of dendritic spines from CA1 neurons of wild-type and MAP1B+/− organotypic hippocampal slice cultures expressing EGFP-actin. Scale bar: 2 µm. (**B**) Cumulative probability distribution of spine/dendrite ratios of EGFP-actin fluorescence in MAP1B+/+ and MAP1B+/− dendritic spines. '*n*' represents the number of spine–dendrite pairs. '*P*' represents the statistical significance value according to the Kolmogorov–Smirnov test. (**C**) Average spine/dendrite ratio of EGFP-actin fluorescence from wild-type and MAP1B+/− dendritic spines. '*n*' represents the number of dendrites. '*P*' represents the statistical significance value, according to the Mann–Whitney test. (**D**) Representative confocal images of apical dendrites from wild-type and MAP1B+/− CA1 neurons filled with Alexa 594. Scale bar: 2 µm. (**E**) Quantification of average spine density from wild-type and MAP1B+/− neurons. (**F**) Similarly to (**E**), sorting spine density values according to distance to the first dendritic branch. (**G**) Quantification of average spine head diameter from wild-type and MAP1B+/− neurons. For (**E–G**), '*n*' represents the number of animals, with 14 and 21 cells for wild-type and MAP1B+/− animals, respectively. (**H**) Cumulative probability distribution of spine head diameters from the same data as in (**G**). '*n*' represents the number of spines. For all panels, black corresponds to wild type and grey to MAP1B+/−.

To evaluate the synaptic localization of Tiam1, we prepared synaptosomal extracts from the forebrain of wild-type and MAP1B mutant mice, and compared the relative levels of Tiam1, Rac1, PSD95 and MAP1B. As shown in Figure 6, Tiam1 expression in whole-cell homogenates was similar in wild-type and mutant animals. In contrast, Tiam1 accumulation in the synaptosomal fraction was significantly lower (by ~40%) in MAP1B-deficient animals, as compared to wild type. Importantly, PSD95 and Rac1 levels did not change in mutant animals in either homogenate or synaptosomal fraction. As expected, MAP1B expression was significantly reduced in MAP1B+/− animals in both homogenate and synaptosomal fractions (Figure 6). Therefore, these results suggest that MAP1B is a critical factor for the targeting of Tiam1 to synaptic compartments, which may result in impaired Rac1 activation at synapses.

In order to directly test whether insufficient Rac1 activation was responsible for the absence of LTD in MAP1B-deficient neurons, we prepared organotypic hippocampal slices from wild-type or MAP1B+/− animals, and overexpressed wild-type Rac1 in CA1 hippocampal neurons (overexpression of constitutively active Rac1 was toxic in our experimental system). To note, this manipulation did not alter passive membrane properties of wild-type or MAP1B+/− neurons (Supplementary Figure 4A and B). As a control for virus infection and protein overexpression, we used EGFP-expressing neurons, which display similar LTD as uninfected neurons (Supplementary Figure 4C and D). We then tested whether an additional supply of Rac1 would alter NMDAR-dependent LTD (1 Hz stimulation, 15 min). MAP1B+/− neurons overexpressing EGFP showed no significant depression (Figure 7A, green circles), consistent with our data using acute slices (Figure 3). In contrast, MAP1B+/− neurons overexpressing Rac1 showed robust depression, which was significantly different from EGFP-expressing neurons (Figure 7A, red circles). Importantly, this manipulation did not significantly alter LTD expression in wild-type neurons (Figure 7B, green and red circles), implying that the rescue of LTD by the overexpression of Rac1 is specific for the MAP1B-deficient animals.

We have previously shown that MAP1B-deficient neurons also contain abnormally high levels of active RhoA (Montenegro-Venegas *et al*, 2010; Tortosa *et al*, 2011). Therefore, we also tested whether excessive active Rho was responsible for the impairment of LTD in MAP1B-deficient neurons. To this end, we expressed a well-established RhoA dominant-negative mutant (RhoA-DN; Qiu *et al*, 1995) in organotypic slices from wild-type and MAP1B mutant animals. As shown in Figure 7A (blue symbols), inhibition of RhoA activity failed to rescue LTD in MAP1B-deficient neurons, and did not alter normal LTD in wild-type neurons (Figure 7B, blue symbols).

Therefore, these results suggest that insufficient Rac1 activation (but not RhoA overactivation) is the cause of the LTD impairment in MAP1B-deficient neurons, and this deficit can be overcome by supplying additional Rac1 protein.

In addition, we monitored the effect of these small GTPases on AMPAR and NMDAR-mediated synaptic responses in CA1 pyramidal neurons under basal conditions, using whole-cell simultaneous double recordings. Overexpression of Rac1 did not significantly change AMPAR or NMDAR responses compared to control neighbouring neurons in MAP1B+/− mutant (Supplementary Figure 5A and B, red columns) or wild-type (Supplementary Figure 5C and D, red columns) slices. On the other hand, RhoA-DN overexpression significantly decreased AMPAR-mediated responses in MAP1B+/− neurons (Supplementary Figure 5A, blue column), but not in wild-type neurons (Supplementary Figure 5C, blue column), without significant changes in NMDAR responses

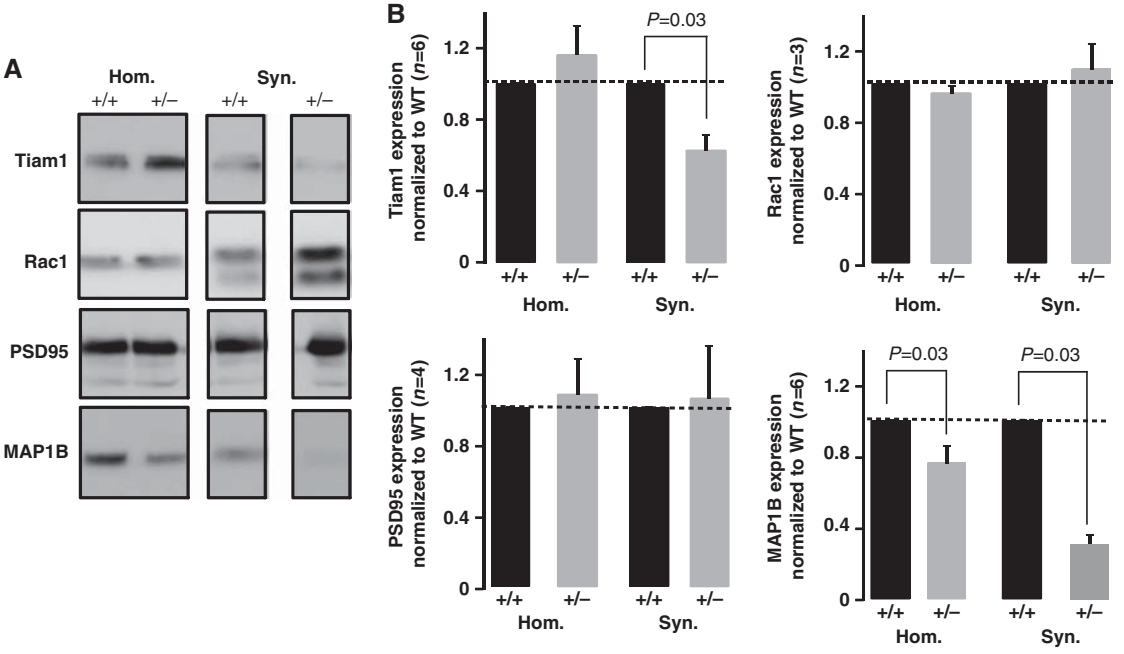

Figure 6 Accumulation of synaptic proteins in MAP1B-deficient neurons. (**A**) Representative western blot of Tiam1, Rac1, PSD95 and MAP1B levels from total homogenates and synaptosomal fraction from wild-type and MAP1B+/− mouse brain. (**B**) Quantification of Tiam1, Rac1, PSD95 and MAP1B levels, normalized to wild-type levels, from experiments as the one shown in (**A**).

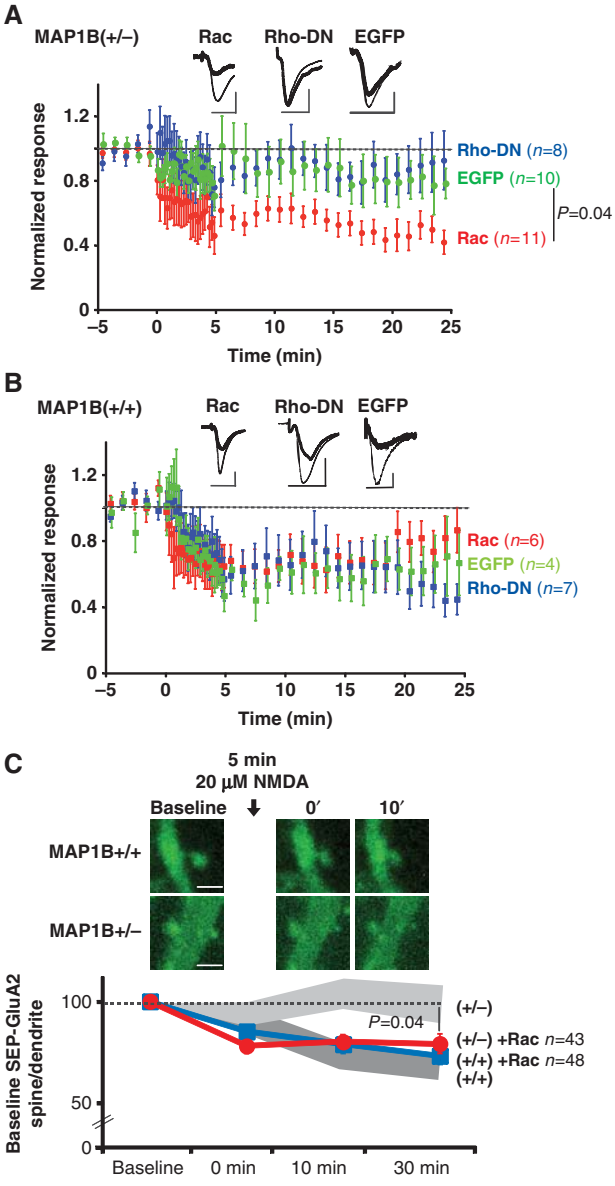

Figure 7 Effect of Rac1 and RhoA-DN on LTD in MAP1B-deficient neurons. (**A**) Time course of NMDAR LTD (300 pulses at 1 Hz) in organotypic hippocampal slices from MAP1B+/− neurons expressing EGFP-Rac1 (red symbols), EGFP-RhoA-DN (blue symbols) or EGFP (green symbols). Inset: sample traces from representative neurons before (thin lines) or after (thick lines) LTD induction. Scale bars correspond to 20 ms and 20 pA. (**B**) Similar to (**A**), with organotypic hippocampal slices from wild-type animals. (**C**) Upper panels: representative confocal images of SEP-GluA2 in dendritic spines from CA1 neurons of wild-type and MAP1B+/− organotypic hippocampal slice cultures expressing SEP-GluA2 and Tomato-Rac1 (not representated). Images were acquired before (Baseline) and at different times after cLTD induction (black arrow, 20 µM NMDA). Scale bar: 2 µm. Lower panel: time course of SEP-GluA2 spine/dendrite ratios normalized to the baseline value for wild-type (blue symbols) and MAP1B+/− (red symbols) neurons. There was a significant decrease in SEP-GluA2 spine/dendrite ratio compared to baseline for wild-type neurons ($P=0.0002$ at 0 min and $P<0.0001$ at 10 and 30 min; Wilcoxon test) and for MAP1B-deficient neuron ($P<0.0001$ at 0, 10 and 30 min; Wilcoxon test). Shadowed bands represent the results shown in Figure 4C for wild-type (dark grey) and MAP1B+/− (light grey) neurons. '*n*' represents the number of spine–dendrite pairs. '*P*' represents the statistical significance value when comparing SEP-GluA2 changes between MAP1B+/− neurons with and without Tomato-Rac1 overexpression (Mann–Whitney test).

(Supplementary Figure 5B and D, blue columns). Therefore, blockade of RhoA activity produces a specific depression of AMPAR responses in MAP1B-deficient neurons. Nevertheless, this effect appears to be independent of LTD, which is only rescued by providing additional Rac activity. As expected, overexpression of EGFP did not change AMPAR or NMDAR-mediated responses in either MAP1B+/− or wild-type neurons (Supplementary Figure 5, green columns).

Rac1 overexpression rescues AMPAR endocytosis in MAP1B-deficient neurons

In order to test whether deficient Rac1 activation is also responsible for the impaired AMPAR endocytosis in MAP1B-deficient neurons, we overexpressed Tomato-Rac1 together with SEP-GluA2 in organotypic slice cultures. Then, AMPAR endocytosis during cLTD was monitored from the decrease in SEP-GluA2 fluorescence, as described for Figure 4A–C.

As shown in Figure 7C, cLTD induction in wild-type neurons produced a reduction in SEP-GluA2 fluorescence (blue symbols), which was very similar to the one observed when Rac1 was not overexpressed (dark grey band, replotted from Figure 4C). This result indicates that GluA2 internalization from the spine surface during LTD proceeds normally on a wild-type background and it is not affected by Rac1 overexpression. In contrast, SEP-GluA2 fluorescence was only significantly decreased in MAP1B+/− neurons when Tomato-Rac1 is overexpressed (Figure 7C, red symbols), whereas this reduction was not observed in the absence of Rac1 overexpression (light grey band, replotted from Figure 4C). This result indicates that AMPARs can be internalized during LTD in MAP1B-deficient neurons when supplying additional Rac1 protein. Therefore, these data strengthen the interpretation that the rescue of LTD by Rac1 in MAP1B-deficient neurons (Figure 7A) is achieved by restoring AMPAR endocytosis.

Discussion

Here, we have showed that MAP1B plays a distinct role during synaptic plasticity, separable from its functions during neuronal development. Specifically, MAP1B is required to provide sufficient Rac1 activation at synapses for the internalization of AMPARs and spine remodelling during LTD. This is based on four main lines of experimental evidence: (1) A reduction in MAP1B levels (MAP1B+/− animals and shRNA) is enough to block NMDAR- and mGluR-dependent LTD. (2) MAP1B deficiency specifically impairs LTD-induced AMPAR endocytosis from the spine surface. (3) Tiam1 synaptic targeting and spine structural plasticity are also impaired in MAP1B-deficient neurons. (4) LTD expression and AMPAR endocytosis are restored by providing additional Rac1 protein in MAP1B-deficient neurons.

This restricted role of MAP1B for LTD is particularly interesting, considering the pleiotropic effects of MAP1B deficiencies in developing neurons. MAP1B knock-out animals are born with profound alterations in the organization of the central nervous system, including a lack of laminar organization in several brain regions and enlargement of cerebral ventricles (Gonzalez-Billault *et al*, 2000). This is consistent with an important role of MAP1B in axonal growth (Gonzalez-Billault *et al*, 2001), neuronal migration and axonal guidance (Del Rio *et al*, 2004). We have

previously shown that MAP1B is important for the maturation of dendritic spines and synaptic transmission in developing neurons (Tortosa *et al*, 2011). Therefore, it is interesting that we found no changes in spine density or morphology, AMPAR- or NMDAR-mediated synaptic transmission in adult MAP1B+/− animals. These results imply that some compensatory mechanisms take place during postnatal development of the animal, such that initial defects in spine morphology and basal synaptic transmission are overcome. Indeed, the upregulation of RhoA activity in these animals (Montenegro-Venegas *et al*, 2010; Tortosa *et al*, 2011) seems to be related to these compensatory mechanisms, since we have observed that blockade of this pathway with a dominant-negative RhoA returns MAP1B-deficient neurons to a state of depressed basal synaptic transmission. We have not explored this effect any further, but it has been shown that RhoA interacts with AMPARs, and Rho activity has been associated with synaptic potentiation and stabilization of the actin cytoskeleton (Schubert *et al*, 2006; Rex *et al*, 2009). In any case, the fact that synaptic transmission and neuronal morphology are unaffected in these adult animals has allowed us to uncover a distinct role of MAP1B in mature neurons, which is the expression of LTD. To note, a previous study has reported deficits in LTP in a different MAP1B+/− mouse model (Zervas *et al*, 2005). However, these animals display a high variability of morphological and neurological phenotypes (Edelmann *et al*, 1996). In contrast, we have observed *enhanced* LTP in MAP1B+/− animals, particularly with weak induction protocols. This may reflect a genuine role of MAP1B in LTP, or alternatively, it may be an indirect consequence of impaired LTD expression. We have not pursued this issue further.

What is the mechanism by which MAP1B participates in LTD? Interestingly, we found that MAP1B is required for triggering the endocytosis of AMPARs from the synaptic membrane after LTD induction. This is surprising because this MAP is only scarcely present at spines (Tortosa *et al*, 2011). A previous report showed that mGluR-dependent AMPAR internalization is impaired in dissociated neuronal cultures after MAP1B siRNA knock-down (Davidkova and Carroll, 2007). However, this study did not evaluate whether initial AMPAR endocytosis or some other downstream event, such as intracellular retention after internalization (Citri *et al*, 2010) or post-endocytic sorting (Fernandez-Monreal *et al*, 2012), was affected. In addition, the mechanism by which MAP1B controls AMPAR internalization remained unclear. By monitoring fluorescently tagged AMPARs at dendritic spines in real time during LTD, we now show that AMPARs remain at the spine plasma membrane from the beginning of LTD induction to the end of the experiment, strongly suggesting that the endocytic process *per se* is defective in MAP1B-deficient neurons. How does an essentially dendritic protein, such as MAP1B, affect endocytosis at the plasma membrane of the spine? We propose that this 'action at a distance' is based on MAP1B's role as a mediator of synaptic Rac activation, which would be achieved by targeting the Rac-GEF Tiam1 to synaptic compartments. This is consistent with the observation that NMDAR activation increases Rac1 activity (Tejada-Simon *et al*, 2006; Xie *et al*, 2007), which in turn is required for LTD expression (Bongmba *et al*, 2011; Martinez and Tejada-Simon, 2011). Interestingly, our data suggest that the interaction MAP1B-Tiam1 is the limiting factor for Rac function during LTD, since we found that simply reducing MAP1B levels by 50% completely abolishes LTD expression. In agreement with the critical importance of MAP1B expression levels, it has been shown that the regulation of MAP1B synthesis correlates with LTD (Davidkova and Carroll, 2007; Chen and Shen, 2013).

The specific role of Rac1, and by extension, actin remodelling in LTD, is far from clear. Rac1 is generally considered as a 'facilitator' of actin polymerization (Ridley *et al*, 1992), and it has been shown to promote AMPAR clustering (Wiens *et al*, 2005). However, LTD is typically associated with actin depolymerization (Okamoto *et al*, 2004). This apparent contradiction is probably the result of the different developmental stages at which remodelling of the actin cytoskeleton by Rac1 takes place. Thus, 'constructive' roles of Rac1 have been typically associated to spinogenesis and synaptic maturation in developing neurons (Tashiro and Yuste, 2004; Wiens *et al*, 2005). Indeed, we have also shown that these processes are altered in a similar manner in MAP1B-deficient animals (Tortosa *et al*, 2011). At later developmental stages, remodelling of different pools of actin and activation of specific signalling pathways during synaptic plasticity may have divergent functional outcomes (Cingolani and Goda, 2008; Shirao and Gonzalez-Billault, 2013). For example, actin polymerization is known to be important for endocytosis (Smythe and Ayscough, 2006), possibly as a inducer of the initial membrane invagination (Kukulski *et al*, 2012). This would explain why AMPARs fail to internalize in MAP1B-deficient neurons. The fact that LTD-induced spine shrinkage is also defective in MAP1B+/− animals may be a consequence of the failure to remove AMPARs (e.g., an AMPAR mutant that cannot be internalized prevents amyloid beta-induced spine loss; Hsieh *et al*, 2006). Alternatively, separate Rac1-dependent mechanisms may operate for the remodelling of the actin cytoskeleton to allow spine shrinkage. This interpretation is consistent with the observation that Rac1 activity is required for changes in spine shape (Tashiro *et al*, 2000; Tashiro and Yuste, 2004).

Irrespective from the details of Rac1's action in LTD, this work has provided mechanistic insight into the regulation of AMPAR trafficking during LTD, and highlights the role of MAPs as signalling platforms for actin remodelling in dendritic spines and changes in synaptic strength during plasticity.

Materials and methods

Ethics statement

All biosafety procedures and animal care protocols were approved by the bioethics committee from the Consejo Superior de Investigaciones Cientificas (CSIC), and were carried out according to the guidelines set out in the European Community Council Directives (86/609/EEC).

DNA constructs and antibodies

The plasmid with EGFP-actin was a generous gift from Francis Castets (Université de la Méditerranée, France). Rac1 and RhoA coding sequences were cloned by PCR from a commercial rat brain cDNA preparation (Clontech). These constructs and EGFP were cloned in pSinRep5 for expression using Sindbis virus (Malinow *et al*, 2010). The Sindbis virus construct for the co-expression of SEP-GluA2 and Tomato was a generous gift from Roberto Malinow (UC San Diego, USA). This construct was modified by PCR to drive

the co-expression of SEP-GluA2 and the Tomato-Rac1 fusion protein. The shRNA against MAP1B (target sequence at position 2012 of the mRNA: 5′-GCCCAAGAAAGAAGTGGTTAA-3′) and the corresponding scrambled sequence (5′-GACATACAGTGAGCGG ATAAA-3′) was expressed using a lentivirus system. Anti-MAP1B and anti-Tiam1 antibodies were from Santa Cruz Biotechnology, anti-Rac1 antibody from BD Biosciences, and anti-PSD95 from Neuromab.

Electrophysiology

Acute slices. Slices of 400 μm-thickness were obtained from 2- to 3-week-old MAP1B+/− mice and wild-type littermates, and maintained in artificial cerebrospinal fluid (ACSF), saturated with 95% O_2/5% CO_2, at room temperature. ACSF consisted of (in mM): 124 NaCl, 2.69 KCl, 26 $NaHCO_3$, 1.25 KH_2PO_4, 10 glucose, 2.5 $CaCl_2$, 1.2 $MgCl_2$, for LTP, LTD and PTP experiments, and 2 $CaCl_2$, 2 $MgCl_2$, for AMPA/NMDA, AMPA/GABA and PPF experiments. After 60 min recovery, slices were placed in the recording chamber. Voltage-clamp recording were obtained from CA1 pyramidal neurons with patch recording pipettes (3–6 MΩ) filled with (in mM) 115 caesium methanesulphonate, 20 CsCl, 10 HEPES, 2.5 $MgCl_2$, 4 disodium ATP, 0.4 trisodium GTP, 10 sodium phosphocreatine and 0.6 EGTA, pH 7.25. Synaptic responses were evoked with bipolar electrodes using single-voltage pulses (up to 30 V or 500 μA). The stimulating electrodes were placed over Schaffer collateral fibres in *stratum radiatum* area. Synaptic AMPAR-mediated responses are measured at −60 mV, NMDAR-mediated responses (in the presence of 0.1 mM picrotoxin) at +40 mV, and $GABA_A$R-mediated responses (in the presence of 0.1 mM AP-V) at 0 mV.

fEPSPs were recorded with glass electrodes (filled with ACSF, 0.8–0.2 MΩ) placed in the apical dendritic layer of CA1 area. PTP was induced in presence of 100 μM AP-V with 100 Hz, 1 s Schaffer collateral stimulation. HFS LTP was induced with 4 trains of 100 Hz, 1 s Schaffer collateral stimulation. TBS LTP was induced with 5 trains of 10 bursts at 5 Hz, each burst consisting of 4 pulses at 100 Hz. In some of the experiments, LTP was induced with the same protocol but with an ACSF containing 2 mM $CaCl_2$, 2 mM $MgCl_2$. NMDAR-dependent LTD was induced with 1 Hz, 900 pulses Schaffer collateral stimulation. mGluR-dependent LTD was induced by perfusing 50 μM (RS)-3,5-dihydroxyphenylglycine (DHPG) for 5 min at 30°C.

Organotypic slices. Organotypic hippocampal slice cultures were infected with Sindbis virus for the expression of recombinant proteins for 24–36 h. Voltage-clamp simultaneous whole-cell recordings were obtained from nearby pairs of infected and uninfected (control) CA1 pyramidal neurons, under visual guidance using fluorescence and transmitted light illumination. The recording chamber was perfused with ACSF, as described above, but containing 4 mM $CaCl_2$, 4 mM $MgCl_2$ and 4 μM 2-chloroadenosine. Patch recording pipettes (3–6 MΩ) were filled as previously described. Synaptic responses were evoked with bipolar electrodes using single-voltage pulses (200 μs, up to 25 V). The stimulating electrodes were placed over Schaffer collateral fibres between 300 and 500 μm from the recorded cells. Because only CA1 cells (and not CA3 cells) were infected, this configuration ensures that recombinant proteins are always expressed exclusively in the postsynaptic cell. NMDAR-dependent LTD was induced by pairing low-frequency presynaptic stimulation (300 or 500 pulses, as indicated, at 1 Hz) with moderate postsynaptic depolarization (−40 mV). Electrophysiological recordings were carried out with Multiclamp 700A/B amplifiers (Molecular Devices) or Microelectrode AC Amplifier Model 1800 (A-M Systems). Data acquisition and analysis was performed with pClamp software or with custom software written in Igor Pro (Wavemetrics).

Hippocampal primary cultures

Hippocampi were dissected from E18 mouse embryos and cells dissociated with trypsin. Neurons were plated onto poly-L-lysine-coated coverslips and cultured in Neurobasal medium supplemented with B27 and glutamine. Cells were maintained at 37°C and 5% CO_2. Neurons were infected with lentivirus driving the expression of the shRNA against MAP1B or the scrambled sequence.

Spine morphology

Slices of 150 μm thickness from paraformaldehyde-perfused 2-month-old wild-type and MAP1B+/− male littermates were used to fill-in CA1 neurons with Alexa 594. Neurons (*stratum radiatum and stratum oriens*) were acquired with a ×63 oil objective and the stacks were deconvoluted to reduce the out-of-focus light. *Vias* and *Neuronstudio* program was used to measure spine density and spine head volume. Dendritic length was determined by tracing each dendritic segment in three dimensions. Spines were marked on the three-dimensional image of each dendrite. Number of spines in each dendritic segment was then divided by the dendritic length to get the spine density. Spine head diameter was calculated tracing a circle corresponding to the perimeter of the spine. Image acquisition and spine quantifications were done blind with respect to the genotype of the animal being analysed.

Confocal fluorescence imaging

Organotypic hippocampal slices (5–7 DIV) expressing different recombinant proteins were perfused with ACSF for 5 min. Fluorescence images were obtained with a Zeiss LSM510 confocal microscope using a ×63 oil immersion objective. Digital images were acquired using Zen software. For chemical LTD experiments, baseline images from dendritic spines were acquired, and then the perfusion solution was switched to an ACSF containing 20 μM NMDA. After 5 min of NMDA treatment, the slices were perfused again with standard ACSF. Images were acquired just after the induction and at different time during the ACSF wash. Images were reconstructed and analysed using NIH Image J software.

Preparation of synaptosomal fractions

Biochemical isolation of crude synaptosomes was carried out essentially as previously described (Carlin *et al*, 1980). Briefly, forebrain from adult mice was homogenized in a Dounce glass homogenizer with buffer A (0.32 M sucrose, 1 mM $MgCl_2$, 0.5 mM $CaCl_2$, 10 mM HEPES, 1 mM EGTA, 1 mM dithiothreitol and a cocktail of protease inhibitors from Roche—'Complete Mini EDTA-free'). This homogenate was spun down at 1400 *g* for 10 min at 4°C. The supernatant was kept and the pellet was resuspended in buffer A and spun again at 710 *g* for 10 min at 4°C. Both supernatants were mixed and spun down at 11 600 *g* for 12 min at 4°C. The pellet (crude synaptosomal fraction) was resuspended in 10 mM HEPES, 1 mM dithiothreitol, 0.32 M sucrose plus a protease inhibitor cocktail. Protein amount was quantified by Bradford and analysed by PAGE–SDS and western blot. Images were analysed using NIH Image J software.

Statistical analyses

All graphs represent average values ± s.e.m. Statistical differences were calculated according to non-parametric tests. For pairwise comparisons, *P*-values were calculated according to two-tailed Mann–Whitney tests (for unpaired data) or Wilcoxon tests (for paired data). Comparisons between cumulative distributions were calculated with the Kolmogorov–Smirnov test.

Supplementary data

Supplementary data are available at *The EMBO Journal* Online (http://www.embojournal.org).

Acknowledgements

We thank C Pitaval for his valuable advice in molecular biology techniques, and the personnel at the fluorescence microscopy facility of the CBMSO (SMOC) for their expert technical assistance. We also thank the members of the Esteban laboratory for their critical reading of the manuscript. The monoclonal antibody against PSD-95 was developed by and obtained from the UC Davis/NIH NeuroMab Facility, supported by NIH grant U24NS050606 and maintained by the Department of Neurobiology, Physiology and Behavior, College of Biological Sciences, University of California, Davis, CA 95616. This work was supported by grants from the Spanish Ministry (SAF-2008-04616, SAF-2009-05558-E, CSD-2010-00045 and SAF-2011-24730), Fundación Ramón Areces and Institute de France-NRJ to JAE; FONDECYT 1120580 to BM; FONDECYT 1095089 to CG-B; VRID-

USACH to PR, and CONICYT ACT-1113 to BM and PR; SAF-2011-24841 to JA. MB and RP are recipients of post- and pre-doctoral contracts, respectively, from the Instituto de Salud Carlos III. MB is also the recipient of an award from the Fondation Bettencourt-Schuller (France).

Author contributions: MB, PR, BM, CG-B and JAE designed research; MB, RP and CR performed research; ET and JA provided mutant mice; MB, RP and CR analysed data; MB and JAE wrote the paper.

Conflict of interest

The authors declare that they have no conflict interest.

References

Beattie EC, Carroll RC, Yu X, Morishita W, Yasuda H, von Zastrow M, Malenka RC (2000) Regulation of AMPA receptor endocytosis by a signaling mechanism shared with LTD. *Nat Neurosci* **3:** 1291–1300

Bongmba OY, Martinez LA, Elhardt ME, Butler K, Tejada-Simon MV (2011) Modulation of dendritic spines and synaptic function by Rac1: a possible link to Fragile X syndrome pathology. *Brain Res* **1399:** 79–95

Brown TC, Tran IC, Backos DS, Esteban JA (2005) NMDA receptor-dependent activation of the small GTPase Rab5 drives the removal of synaptic AMPA receptors during hippocampal LTD. *Neuron* **45:** 81–94

Carlin RK, Grab DJ, Cohen RS, Siekevitz P (1980) Isolation and characterization of postsynaptic densities from various brain regions: enrichment of different types of postsynaptic densities. *J Cell Biol* **86:** 831–845

Cingolani LA, Goda Y (2008) Actin in action: the interplay between the actin cytoskeleton and synaptic efficacy. *Nat Rev Neurosci* **9:** 344–356

Citri A, Bhattacharyya S, Ma C, Morishita W, Fang S, Rizo J, Malenka RC (2010) Calcium binding to PICK1 is essential for the intracellular retention of AMPA receptors underlying long-term depression. *J Neurosci* **30:** 16437–16452

Colledge M, Snyder EM, Crozier RA, Soderling JA, Jin Y, Langeberg LK, Lu H, Bear MF, Scott JD (2003) Ubiquitination regulates PSD-95 degradation and AMPA receptor surface expression. *Neuron* **40:** 595–607

Chen YL, Shen CK (2013) Modulation of mGluR-dependent MAP1B translation and AMPA receptor endocytosis by microRNA miR-146a-5p. *J Neurosci* **33:** 9013–9020

Davidkova G, Carroll RC (2007) Characterization of the role of microtubule-associated protein 1B in metabotropic glutamate receptor-mediated endocytosis of AMPA receptors in hippocampus. *J Neurosci* **27:** 13273–13278

Del Rio JA, Gonzalez-Billault C, Urena JM, Jimenez EM, Barallobre MJ, Pascual M, Pujadas L, Simo S, La Torre A, Wandosell F, Avila J, Soriano E (2004) MAP1B is required for Netrin 1 signaling in neuronal migration and axonal guidance. *Curr Biol* **14:** 840–850

Edelmann W, Zervas M, Costello P, Roback L, Fischer I, Hammarback JA, Cowan N, Davies P, Wainer B, Kucherlapati R (1996) Neuronal abnormalities in microtubule-associated protein 1B mutant mice. *Proc Natl Acad Sci USA* **93:** 1270–1275

Fernandez-Monreal M, Brown TC, Royo M, Esteban JA (2012) The balance between receptor recycling and trafficking toward lysosomes determines synaptic strength during long-term depression. *J Neurosci* **32:** 13200–13205

Gonzalez-Billault C, Avila J (2000) Molecular genetic approaches to microtubule-associated protein function. *Histol Histopathol* **15:** 1177–1183

Gonzalez-Billault C, Avila J, Caceres A (2001) Evidence for the role of MAP1B in axon formation. *Mol Biol Cell* **12:** 2087–2098

Gonzalez-Billault C, Demandt E, Wandosell F, Torres M, Bonaldo P, Stoykova A, Chowdhury K, Gruss P, Avila J, Sanchez MP (2000) Perinatal lethality of microtubule-associated protein 1B-deficient mice expressing alternative isoforms of the protein at low levels. *Mol Cell Neurosci* **16:** 408–421

Gonzalez-Billault C, Jimenez-Mateos EM, Caceres A, Diaz-Nido J, Wandosell F, Avila J (2004) Microtubule-associated protein 1B function during normal development, regeneration, and pathological conditions in the nervous system. *J Neurobiol* **58:** 48–59

Gonzalez-Billault C, Owen R, Gordon-Weeks PR, Avila J (2002) Microtubule-associated protein 1B is involved in the initial stages of axonogenesis in peripheral nervous system cultured neurons. *Brain Res* **943:** 56–67

Halpain S, Dehmelt L (2006) The MAP1 family of microtubule-associated proteins. *Genome Biol* **7:** 224

Henriquez DR, Bodaleo FJ, Montenegro-Venegas C, Gonzalez-Billault C (2012) The light chain 1 subunit of the microtubule-associated protein 1B (MAP1B) is responsible for Tiam1 binding and Rac1 activation in neuronal cells. *PLoS One* **7:** e53123

Horne EA, Dell'Acqua ML (2007) Phospholipase C is required for changes in postsynaptic structure and function associated with NMDA receptor-dependent long-term depression. *J Neurosci* **27:** 3523–3534

Hsieh H, Boehm J, Sato C, Iwatsubo T, Tomita T, Sisodia S, Malinow R (2006) AMPAR removal underlies Abeta-induced synaptic depression and dendritic spine loss. *Neuron* **52:** 831–843

Hu X, Viesselmann C, Nam S, Merriam E, Dent EW (2008) Activity-dependent dynamic microtubule invasion of dendritic spines. *J Neurosci* **28:** 13094–13105

Jaworski J, Kapitein LC, Gouveia SM, Dortland BR, Wulf PS, Grigoriev I, Camera P, Spangler SA, Di Stefano P, Demmers J, Krugers H, Defilippi P, Akhmanova A, Hoogenraad CC (2009) Dynamic microtubules regulate dendritic spine morphology and synaptic plasticity. *Neuron* **61:** 85–100

Kang MG, Guo Y, Huganir RL (2009) AMPA receptor and GEF-H1/Lfc complex regulates dendritic spine development through RhoA signaling cascade. *Proc Natl Acad Sci USA* **106:** 3549–3554

Kim MJ, Futai K, Jo J, Hayashi Y, Cho K, Sheng M (2007) Synaptic accumulation of PSD-95 and synaptic function regulated by phosphorylation of serine-295 of PSD-95. *Neuron* **56:** 488–502

Kukulski W, Schorb M, Kaksonen M, Briggs JA (2012) Plasma membrane reshaping during endocytosis is revealed by time-resolved electron tomography. *Cell* **150:** 508–520

Makino H, Malinow R (2009) AMPA receptor incorporation into synapses during LTP: the role of lateral movement and exocytosis. *Neuron* **64:** 381–390

Malinow R, Hayashi Y, Maletic-Savatic M, Zaman SH, Poncer JC, Shi SH, Esteban JA, Osten P, Seidenman K (2010) Introduction of green fluorescent protein (GFP) into hippocampal neurons through viral infection. *Cold Spring Harb Protoc* **2010:** pdb.prot5406

Malinow R, Malenka RC (2002) AMPA receptor trafficking and synaptic plasticity. *Annu Rev Neurosci* **25:** 103–126

Martinez LA, Tejada-Simon MV (2011) Pharmacological inactivation of the small GTPase Rac1 impairs long-term plasticity in the mouse hippocampus. *Neuropharmacology* **61:** 305–312

Meixner A, Haverkamp S, Wassle H, Fuhrer S, Thalhammer J, Kropf N, Bittner RE, Lassmann H, Wiche G, Propst F (2000) MAP1B is required for axon guidance and Is involved in the development of the central and peripheral nervous system. *J Cell Biol* **151:** 1169–1178

Merriam EB, Lumbard DC, Viesselmann C, Ballweg J, Stevenson M, Pietila L, Hu X, Dent EW (2011) Dynamic microtubules promote synaptic NMDA receptor-dependent spine enlargement. *PLoS One* **6:** e27688

Montenegro-Venegas C, Tortosa E, Rosso S, Peretti D, Bollati F, Bisbal M, Jausoro I, Avila J, Caceres A, Gonzalez-Billault C (2010) MAP1B regulates axonal development by modulating Rho-GTPase Rac1 activity. *Mol Biol Cell* **21:** 3518–3528

Morishita W, Connor JH, Xia H, Quinlan EM, Shenolikar S, Malenka RC (2001) Regulation of synaptic strength by protein phosphatase 1. *Neuron* **32:** 1133–1148

Mulkey RM, Endo S, Shenolikar S, Malenka RC (1994) Involvement of a calcineurin/inhibitor-1 phosphatase cascade in hippocampal long-term depression. *Nature* **369:** 486–488

Mulkey RM, Herron CE, Malenka RC (1993) An essential role for protein phosphatases in hippocampal long-term depression. *Science* **261:** 1051–1055

Nakamura Y, Wood CL, Patton AP, Jaafari N, Henley JM, Mellor JR, Hanley JG (2011) PICK1 inhibition of the Arp2/3 complex controls dendritic spine size and synaptic plasticity. *EMBO J* **30:** 719–730

Okamoto K, Nagai T, Miyawaki A, Hayashi Y (2004) Rapid and persistent modulation of actin dynamics regulates postsynaptic reorganization underlying bidirectional plasticity. *Nat Neurosci* **7:** 1104–1112

Qiu RG, Chen J, McCormick F, Symons M (1995) A role for Rho in Ras transformation. *Proc Natl Acad Sci USA* **92:** 11781–11785

Rex CS, Chen LY, Sharma A, Liu J, Babayan AH, Gall CM, Lynch G (2009) Different Rho GTPase-dependent signaling pathways initiate sequential steps in the consolidation of long-term potentiation. *J Cell Biol* **186:** 85–97

Ridley AJ (2006) Rho GTPases and actin dynamics in membrane protrusions and vesicle trafficking. *Trends Cell Biol* **16:** 522–529

Ridley AJ, Paterson HF, Johnston CL, Diekmann D, Hall A (1992) The small GTP-binding protein rac regulates growth factor-induced membrane ruffling. *Cell* **70:** 401–410

Schoenfeld TA, McKerracher L, Obar R, Vallee RB (1989) MAP 1A and MAP 1B are structurally related microtubule associated proteins with distinct developmental patterns in the CNS. *J Neurosci* **9:** 1712–1730

Schubert V, Da Silva JS, Dotti CG (2006) Localized recruitment and activation of RhoA underlies dendritic spine morphology in a glutamate receptor-dependent manner. *J Cell Biol* **172:** 453–467

Shirao T, Gonzalez-Billault C (2013) Actin filaments and microtubules in dendritic spines. *J Neurochem* **126:** 155–164

Smythe E, Ayscough KR (2006) Actin regulation in endocytosis. *J Cell Sci* **119:** 4589–4598

Tashiro A, Minden A, Yuste R (2000) Regulation of dendritic spine morphology by the rho family of small GTPases: antagonistic roles of Rac and Rho. *Cereb Cortex* **10:** 927–938

Tashiro A, Yuste R (2004) Regulation of dendritic spine motility and stability by Rac1 and Rho kinase: evidence for two forms of spine motility. *Mol Cell Neurosci* **26:** 429–440

Tejada-Simon MV, Villasana LE, Serrano F, Klann E (2006) NMDA receptor activation induces translocation and activation of Rac in mouse hippocampal area CA1. *Biochem Biophys Res Commun* **343:** 504–512

Tortosa E, Montenegro-Venegas C, Benoist M, Hartel S, Gonzalez-Billault C, Esteban JA, Avila J (2011) Microtubule-associated protein 1B (MAP1B) is required for dendritic spine development and synaptic maturation. *J Biol Chem* **286:** 40638–40648

Tymanskyj SR, Scales TM, Gordon-Weeks PR (2012) MAP1B enhances microtubule assembly rates and axon extension rates in developing neurons. *Mol Cell Neurosci* **49:** 110–119

Wiens KM, Lin H, Liao D (2005) Rac1 induces the clustering of AMPA receptors during spinogenesis. *J Neurosci* **25:** 10627–10636

Xie Z, Srivastava DP, Photowala H, Kai L, Cahill ME, Woolfrey KM, Shum CY, Surmeier DJ, Penzes P (2007) Kalirin-7 controls activity-dependent structural and functional plasticity of dendritic spines. *Neuron* **56:** 640–656

Zervas M, Opitz T, Edelmann W, Wainer B, Kucherlapati R, Stanton PK (2005) Impaired hippocampal long-term potentiation in microtubule-associated protein 1B-deficient mice. *J Neurosci Res* **82:** 83–92

Zhang H, Macara IG (2006) The polarity protein PAR-3 and TIAM1 cooperate in dendritic spine morphogenesis. *Nat Cell Biol* **8:** 227–237

Zhou Q, Homma KJ, Poo MM (2004) Shrinkage of dendritic spines associated with long-term depression of hippocampal synapses. *Neuron* **44:** 749–757